

# A fully automated hot-wall multiplasma-monochamber reactor for thin film deposition

P. Roca i Cabarrocas, J. B. Chévrier, J. Huc, A. Lloret, J. Y. Parey, and J. P. M. Schmitt<sup>a)</sup>  
*Laboratoire de Physique des Interfaces et des Couches Minces (UPR 0258 du CNRS) Ecole Polytechnique,  
F-91128 Palaiseau Cédex, France*

(Received 15 August 1990; accepted 1 December 1990)

We present a study on the development and the evaluation of a fully automated radio-frequency glow discharge system devoted to the deposition of amorphous thin film semiconductors and insulators. The following aspects were carefully addressed in the design of the reactor: (1) cross contamination by dopants and unstable gases, (2) capability of a fully automated operation, (3) precise control of the discharge parameters, particularly the substrate temperature, and (4) high chemical purity. The new reactor, named ARCAM, is a multiplasma-monochamber system consisting of three separated plasma chambers located inside the same isothermal vacuum vessel. Thus, the system benefits from the advantages of multichamber systems but keeps the simplicity and low cost of monochamber systems. The evaluation of the reactor performances showed that the oven-like structure combined with a differential dynamic pumping provides a high chemical purity in the deposition chamber. Moreover, the studies of the effects associated with the plasma recycling of material from the walls and of the thermal decomposition of diborane showed that the multiplasma-monochamber design is efficient for the production of abrupt interfaces in hydrogenated amorphous silicon (*a*-Si:H) based devices. Also, special attention was paid to the optimization of plasma conditions for the deposition of low density of states *a*-Si:H. Hence, we also present the results concerning the effects of the geometry, the substrate temperature, the radio frequency power and the silane pressure on the properties of the *a*-Si:H films. In particular, we found that a low density of states *a*-Si:H can be deposited at a wide range of substrate temperatures ( $100\text{ }^{\circ}\text{C} \leq T_s \leq 300\text{ }^{\circ}\text{C}$ ).

## I. INTRODUCTION

The technology of thin films produced by plasma enhanced chemical vapor deposition processes (PECVD) has experienced a fast development in the last decades.<sup>1,2</sup> In particular, since the discovery of the semiconducting properties of hydrogenated amorphous silicon,<sup>3</sup> extensive progress was accomplished in physics<sup>4</sup> as well as in the development of the applications of this material and related alloys<sup>5</sup> [silicon-germanium (*a*-SiGe:H), silicon-carbide (*a*-SiC:H), silicon-nitride (*a*-SiN:H),...]. Concurrently, several techniques were developed for the deposition of device quality *a*-Si:H,<sup>6</sup> but, because of its easy implantation and its possibility of being scaled up, PECVD is the most widely used technique in laboratory research as well as in industrial applications.

In PECVD the dissociation of the reactive gases is achieved in a capacitively coupled radio-frequency (rf) (13.56 MHz) glow discharge which satisfies the requirements of the versatility necessary for the fabrication of devices. This process often consists in the accumulation of many sequential elementary operations. Thus, in *a*-Si:H based solar cells for example, the *p* layer generally consists of a thin, boron-doped, silicon-carbide alloy (*a*-SiC:H) followed by a buffer layer of intrinsic *a*-SiC:H.<sup>7,8</sup> The electronic properties of *a*-SiC:H alloys have been improved by the combination of 4–12 s of plasma deposition followed by 0–30 s of hydrogen plasma etching;<sup>9</sup> the solar cell efficiency has been increased by even more elaborated processes, such as the use of multilayer structures.<sup>10,11</sup> Also, the interest in

amorphous multilayers and superlattices has increased in the last year.<sup>4</sup> As a consequence, a fully automated operation is more indispensable than ever for a good control and reproducibility of the processes involved in thin film deposition and etching.

Of course, besides the automated processing, the reactor design should satisfy the requirements for production of high-performance thin film devices. In many amorphous thin film device applications (solar cells, thin film transistors, photodetectors,...), these requirements can be specified as follows:

(i) Precise control of the process parameters: gas flow rates, gas pressure, rf power, and substrate temperature. Indeed, the optimization of the deposition conditions, their reproducibility, and the comparison of the results from different laboratories are only possible if the process parameters are known with precision. But as some process parameters are interdependent (see Sec. IV A for the gas pressure and substrate temperature), the optimization of the deposition conditions can be misleading unless a careful measurement of each variable is done.

(ii) Reduced outgassing and impurities: Precise control of the deposition parameters alone does not guarantee the reproducibility of the electronic properties of the deposited films. Indeed as the electronic properties of semiconductors are greatly altered by the incorporation of small amounts of impurities (less than one part per million),<sup>12</sup> the reduction of these impurities (outgassing) is of primary importance.

(iii) Production of a low defect density material. In the case of *a*-Si:H for example, a  $N_s \leq 10^{16}\text{ cm}^{-3}$  is necessary to

allow doping and efficient operation of *a*-Si:H based devices.

(iv) Possibility of doping (*p* type and *n* type) and alloying (*a*-SiGe:H, *a*-SiC:H,...). Doping is the key element which makes the device fabrication possible. Alloying allows to tailor the optical gap of the semiconductors as a function of the applications. For example, by introducing *a*-SiC:H and *a*-SiGe:H alloys one expects to raise the efficiency up to 21.5% in tandem amorphous thin film solar cells.<sup>13</sup>

(v) Production of sharp interfaces. As very thin layers are involved in most of the applications of thin film semiconductors, the ability to produce sharp interfaces is of crucial importance to obtain a proper device operation.

We present in this paper our response to these requirements in terms of reactor design for amorphous thin film device production.

## II. APPARATUS DESIGN

### A. The ARCAM reactor

The "ARCAM" reactor,<sup>14</sup> represented in Fig. 1, consists of a single vacuum vessel containing three independent plasma chambers. The vacuum vessel is a 400-mm diam stainless steel cylinder. Its bottom face contains a centered DN 63 pumping port, the gas input, and the rf electrical connections for each plasma chamber. The cover can be removed for loading operations and is equipped with a water-cooled viton seal. This face is also provided with a rotating feed through connecting a stepping motor to a rotating plate described below. The whole vacuum vessel can be heated up to 300 °C by an oven-like structure made of self-regulated Thermo-coax wires. A protecting thermal isolation surrounds the whole vacuum chamber minimizing the thermal losses. Even though the top, the walls and the cover parts of the reactor are independently heated, the temperature for the three parts is usually set at the same value. As a matter of fact, the reactor is always heated at the desired substrate temperature and kept at a vacuum limit pressure of  $2 \times 10^{-5}$  Pa.

Each plasma chamber consists of a rf electrode disk surrounded by a grounded cylinder (150-mm diam) covered by a disk containing an upper 100-mm diam opening for lateral gas pumping and constituting the window for substrate coating. The electrodes can easily be removed and even modified for the changing of geometrical parameters. Results presented here concern an electrode-to-substrate gap of 28 mm and two values of the rf electrode diameter: 148 and 110 mm, which result in an effective ratio of the rf electrode area  $S_{rf}$  and grounded surface area  $S_g$  of  $S_{rf}/S_g \sim 0.54$  for the former and  $S_{rf}/S_g \sim 0.25$  for the latter. In the following, these two geometries will be named geometry *A* and geometry *B* respectively. The gas flows from the inlet hole centered in the internal face of the rf electrode to the upper-side aperture of the plasma chamber and to the pumping port through a 2-mm gap constituted by the upper part of the plasma chamber and the rotating substrate holder. This annular flow restriction creates a positive differential pressure ( $1 < \Delta P < 13$  Pa) between the plasma chamber and the vacuum vessel and thus reduces chemical contamination during deposition. For an established flow rate, the gas pressure in the vacuum

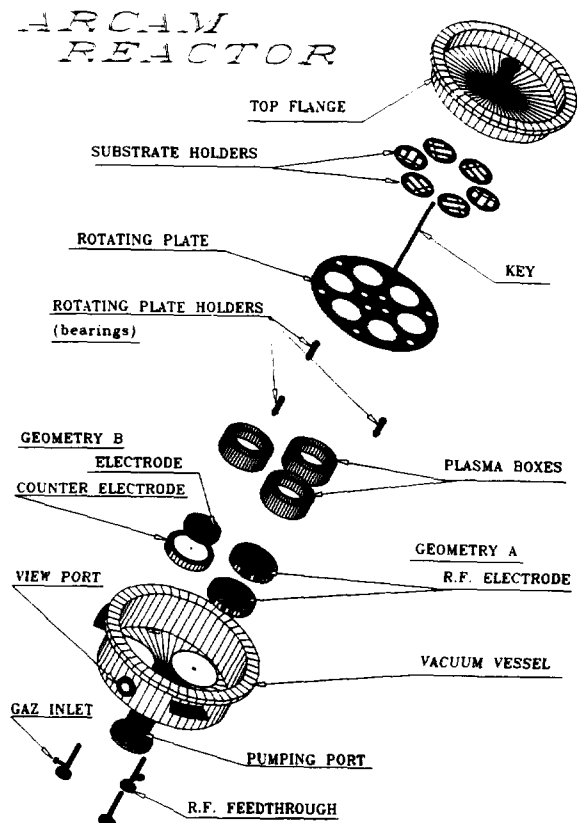


FIG. 1. Exploded view of the ARCAM reactor. The heating system and the stepping motor are not shown for the clarity of the drawing.

chamber is regulated by an electrically driven throttle valve type IB 063 from Balzers. Penning and capacitive pressure sensors are placed in the exhaust lines close to the vacuum chamber and before the throttle valve. A calibration was performed to determine, for a given flow rate and position of the throttle valve, the actual gas pressure in the process chamber.

A stepping motor drives a rotating plate provided with six 100-mm diam substrate locations allowing a large sample production without the vacuum being broken. One of these locations is normally sacrificed for the ignition of the silane plasma and to precoat the plasma chambers. In this way we can further reduce the impurity concentration or the cross contamination in the deposition chamber and avoid the plasma transients on the substrates.<sup>15,16</sup>

### B. Gas handling and pumping

The gas handling system consists of seven lines for reactive gases: silane ( $\text{SiH}_4$ ), germane ( $\text{GeH}_4$ ), methane ( $\text{CH}_4$ ), phosphine ( $\text{PH}_3$ ), diborane ( $\text{B}_2\text{H}_6$ ), hydrogen ( $\text{H}_2$ ), and ammonia ( $\text{NH}_3$ ). Gas contamination sources such as traps in connections, tubes and other components were carefully avoided. The high pressure gas handling and the gas tanks are located in an independent storage room open to the air. The low pressure gas handling and the reactor are inside a highly ventilated glass casing located in a well ventilated working room. The gas handling is based on the

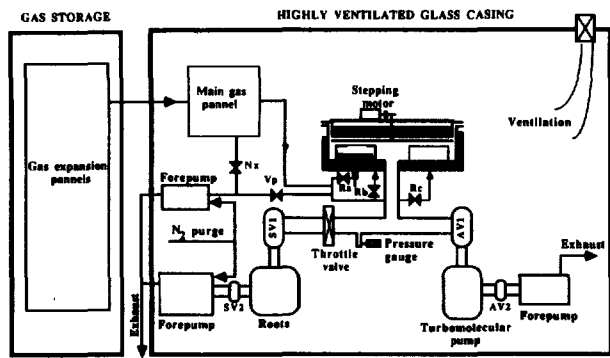


FIG. 2. Schematic view of the gas handling and vacuum systems of the ARCAM reactor.

use of an always dynamic flow to avoid the effects of gas stagnation. For that, before their flow to the deposition chamber, the reactive gases are flowed to the exhaust through an auxiliary primary pump. Valves are three-way and four-way ASM bellows, normally closed, with a reduced dead volume. All the tube connections of the low gas pressure panel are welded and all the components were specially cleaned. The low pressure gas lines are protected by a filter provided by a membrane with 0.2 μm pores and equipped with mass flow controllers by ASM or TYLAN. All the lines for reactive gases can be purged with an independent argon gas line.

The reactor is equipped with two independent pumping systems as shown in Fig. 2. After the opening of the reactor to the air and the loading of the substrates, a turbomolecular pump unit type 5400 from Alcatel and its associated fore-pump type 2012 CP1 are operated until a low gas pressure of  $2 \times 10^{-5}$  Pa is achieved. At this stage the high vacuum level system can be switched off and the reactive gases fed into the reactor. When a pressure setting point of  $\sim 10^{-1}$  Pa is reached, the connecting valve to a Balzers roots blower type WKP 500 SP and a plasma series forepump type 2063 CP1 from Alcatel are automatically opened. We thus prevent oil diffusing back into the deposition chambers. For a given gas flow, the pressure in the deposition chamber is obtained by acting on the throttle valve, whereafter the discharge is established on an empty substrate holder location. This allows for a 10 min  $\alpha$ -Si:H precoating of the plasma chamber walls to bury contaminating molecules and also avoids the transient effects in the lighting of the plasma. After these operations, a substrate is placed over the plasma chamber and deposition started without plasma interruption.

**C. The rf generator**

Dissociation of the reactive gases for the deposition of  $\alpha$ -Si:H and related alloys is achieved through their excitation in a 13.56 MHz capacitively coupled radio-frequency discharge. The power source consists of an rf generator from Nextral producing an adjustable rf power from 0–25 W when matched to a 50 Ω load. As the plasma behaves like a complex impedance, an automatic matching network type RA 30 from Nextral is associated with the rf generator to

ensure that the reflected power is zero in all the discharge conditions. The rf power is distributed to one of the three process chambers by means of a four-way high-voltage rf switch. Only one plasma chamber is switched on at the same time.

**D. System operation**

The apparatus can be operated manually or automatically. After the loading of the substrates, the turbomolecular pump unit is manually triggered. A vacuum limit of  $10^{-4}$  Pa has to be reached before any introduction of reactive gases. In the manual procedure, when the security conditions are satisfied, the gas handling system is operated by means of an IBM PC and Serial interface. In the automatic procedure, when the high vacuum and security conditions are satisfied, all operations (valves, mass flow controllers, stepping motor, rf power, matching, and relay activations), are monitored following a program and controlled in real time by computer. Figure 3 summarizes the systems involved in the operation and control of the deposition system.

**E. The safety of the reactor**

The major safety problems originate from the use of hydride gases because of their high toxicity and flammability. Because of their toxicity the dopant gases are highly diluted with hydrogen (2%) and hydrogen detectors are located close to the reactor and gas handling. The alarm is triggered at 500 ppm of H<sub>2</sub> corresponding to a 10 ppm of dopant gas. In case of alarm, when the safety valves on the gas tanks close, the maximum concentration of phosphine or diborane in the highly ventilated working room is less than 2 ppm. Moreover, independently of the recommended safety norms for industrial uses of hydrides,<sup>17</sup> two security levels have been provided (Fig. 3).

(i) Pumping systems are activated by manual interlocked push buttons. Wrong operator manipulations are avoided and apparatus failures are detected by an electronic pro-

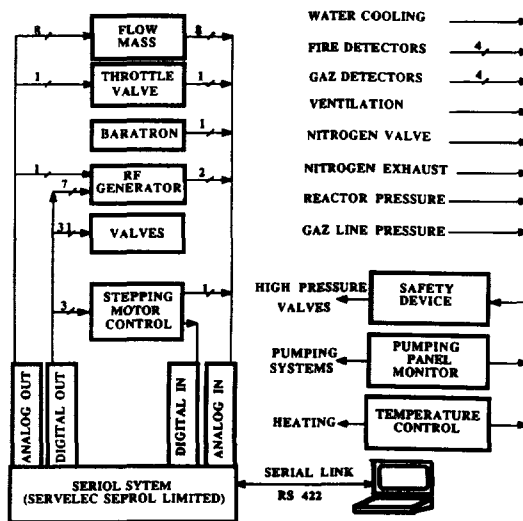


FIG. 3. Schematic diagram of the systems involved in the operation, the control of the process, and the safety of the deposition system.

grammable module built around a read only memory (ROM) which contains the only allowed operation sequences. All valves and pumps are wired with feedback informations monitoring their state. Hardware trouble shooting is transmitted to a safety device, the second level.

(ii) The safety device module monitors in real time up to 16 incoming sets of information, including gas and fire detectors as well as pressure gauges in different parts of the apparatus. In case of over-range measurement all the safety valves are switched off and the reason of the failure is memorized. The automated operation together with the safety devices allows the reactor to operate overnight or during week-ends.

### III. THE AUXILIARY ONE-PLASMA REACTORS

Using *in situ* techniques to characterize the plasma (mass spectrometry, optical emission spectroscopy,...), and to measure the film properties (spectroscopic ellipsometry, Kelvin probe,...) is extremely helpful to obtain a clear correlation between the plasma conditions and the optoelectronic properties of the films. However, setting up these *in situ* techniques is almost incompatible with the high purity required for the deposition of thin film semiconductors. Therefore, four auxiliary single-chamber reactors were built to characterize the plasma and the growth processes used in the ARCAM reactor. The discharge geometry of the auxiliary reactors was chosen to be strictly similar to an individual plasma chamber of the ARCAM, which makes it easier to correlate observations between the experimental reactors and the ARCAM. The only differences between the ARCAM and the auxiliary reactors are the position of the electrodes (horizontal in the ARCAM and vertical in the auxiliary reactors) and the substrate heating: the ARCAM is oven-like whereas in the auxiliary plasma reactors only the substrate holder is heated.

### IV. EVALUATION OF THE SPECIFIC FEATURES OF THE ARCAM REACTOR

#### A. Dynamic differential pressure and hot walls

The hot walls of the ARCAM reactor as well as its differential pumping are two key elements in the obtaining of a high purity in the deposition chamber.

#### 1. Control of the substrate temperature

Among the parameters controlling the quality of *a*-Si:H films, the substrate temperature is critical as it determines the incorporation of hydrogen and the electronic properties of the deposited films (see Sec. V C). It is obvious that a precise control of the substrate temperature is essential to the correlation of the plasma conditions to *a*-Si:H quality and also to the comparison of the properties of films deposited in different reactors. However, the control of the substrate temperature is extremely difficult in the conventional systems where only the substrate holder is heated. In Fig. 4 we present the results of a careful calibration of the substrate temperature as a function of the gas pressure, performed in one of the auxiliary reactors. The regulation temperature of the substrate holder was set at 200 °C, whereas the actual

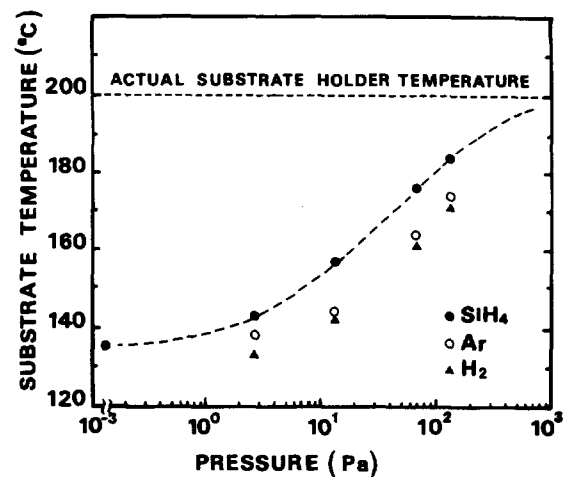


FIG. 4. Measurements of a glass substrate temperature as a function of the gas pressure and for different gases in a system where only the backing plate is heated at the nominal temperature of 200 °C, the rest of the chamber being neither heated nor cooled.

substrate temperature was monitored by a Pt-100 resistor deposited on the top of a glass substrate, generally used in *a*-Si:H depositions. The results presented in Fig. 4 clearly show that it is hard to know the real substrate temperature (thus to compare conditions in which different gas compositions or pressures are used) unless a calibration of the substrate temperature is performed for each deposition condition. We note that these effects become more important as the substrate temperature is set at a higher value. A similar calibration performed in the oven-like heated ARCAM reactor did not show any effect of the gas pressure or gas composition.

Another drawback of just using a substrate holder heating system and not an oven structure is reflected in the results presented in Fig. 4. Indeed, two effects are associated with the pressure dependence of the substrate temperature. On one hand, stopping of the gas flow after deposition of an *a*-Si:H film implies that fast cooling is applied to the substrate. On the other hand, the opening of the reactor to the atmospheric pressure when the substrate holder is still at the regulation temperature will result in an annealing of the sample at the regulation temperature, which for a regulation temperature of 200 °C and a silane pressure of 13.3 Pa is 40 °C higher than the deposition temperature. As a consequence, irreversible effects can be produced in the *a*-Si:H films, in particular when these annealing and fast-cooling effects cross over the equilibrium temperature of the semiconductor.<sup>18,19</sup> Moreover, the substrate temperature in vacuum results from the equalization of radiative heat transfer between the heated substrate holder and the walls of the reactor which are at room temperature. As a consequence the equilibration temperature depends on the emissivity of the substrate and a simple calculation shows that the equilibration temperature of different substrates can differ by more than 50 °C.<sup>20,21</sup>

#### 2. Chemical purity

Control of impurities in the reactor is of primary importance in the deposition of *a*-Si:H with a low density of states.

To obtain high purity, special efforts were made on constructing the gas handling system. However, once in the reactor, the gas composition results from the equilibrium between the chemical purity of the reactive gases and the outgassing from the walls of the reactor. It is clear that the outgassing has to be reduced as much as possible in order to increase the process-gas/outgassing ratio. This can be achieved by the use of a hot wall system in which the outgassing is rapidly obtained as no cold points, with long outgassing periods, exist. To further reduce the impurity concentration in the *a*-Si:H film, the specific design of the process chamber is of crucial importance. As shown in Fig. 1, the gases are fed through the central electrode and get out through the small gap between the plasma chamber and the rotating substrate holder. This results in a differential pressure between the inside of the plasma chamber and the whole vacuum vessel and thus in a reduction of the impurities in the deposition chamber. Indeed, secondary ion mass spectroscopy (SIMS) measurements showed that the oxygen content of *a*-Si:H films is reduced by a factor of 40 through the use of the differential dynamic pumping setup.<sup>22</sup> We present in Table I the results of SIMS measurements concerning the impurity content of *a*-Si:H films deposited in different kind of reactors.<sup>12,23,24</sup> One observes that oxygen, carbon and nitrogen impurities are lower in the ARCAM reactor than in standard monochamber systems.

## B. Multiplasma in a single chamber

Control of the interfaces is of crucial importance for the deposition of thin film semiconductor devices. In the case of *a*-Si:H based solar cells for example, it is the quality of the *p*-*i* interface which largely controls the cell efficiency.<sup>25</sup> As a consequence we paid special attention to the efficiency of the multiplasma-monochamber reactor from the point of view of cross contamination.

### 1. Plasma etching of the material on the walls

The silane plasma is a reactive environment where deposition takes place at the same time as the etching and the sputtering of the material deposited on the walls of the reactor. These effects may produce a cross contamination between the different layers constituting a device when deposited in a monochamber system. In *p*-*i*-*n* *a*-Si:H based solar cells for example, traces of boron from the deposition of the *p* layer may be incorporated in the intrinsic layer and deteriorate its quality. Figure 5 shows the boron concentration pro-

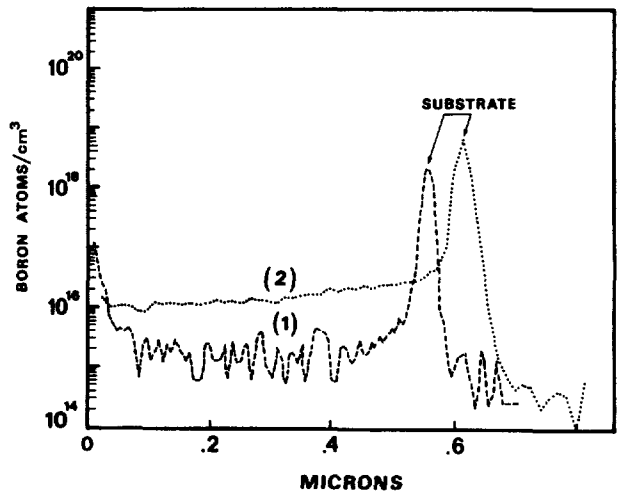


FIG. 5. Boron concentration profiles, determined from SIMS measurements, in two standard intrinsic *a*-Si:H films deposited in a clean (1) and in a boron contaminated chamber (2).

file determined by SIMS in two intrinsic *a*-Si:H samples produced in a clean (1) or in a boron-contaminated chamber (2). The boron concentration is a factor of 10 higher in the film deposited in the *p* chamber, even after a 0.6  $\mu\text{m}$  (2 h) *a*-Si:H deposition. These results clearly show the benefit of a multiplasma system where the plasma recycling of the boron is avoided by the use of three separated plasma chambers.

### 2. Adsorption and thermal decomposition of reactive gases

Control of the adsorption and thermal decomposition of the gases is a key parameter in the production of abrupt interfaces. For example, it has been reported that  $\text{NH}_3$  is strongly adsorbed by the walls of the reactor;<sup>26</sup> as a consequence, it is difficult to obtain sharp interfaces between *a*-Si:H and *a*-SiN:H. Also, the thermal decomposition of the reactive gases on the hot surfaces can be a handicap as it will produce a contamination source in all the hot parts of the reactor.

As phosphine and diborane are the gases we use for *a*-Si:H doping, we studied the effects of the exposing of freshly deposited *a*-Si:H samples and of the reactor walls to silane-phosphine or silane-diborane mixtures. As no physical separation exists between the three deposition chambers of the ARCAM, the gases fed into the *n* or *p* chamber can flow to the *i* chamber and contaminate it. Moreover, they can produce contamination on the *a*-Si:H samples firstly deposited in a series without the breaking of the vacuum. To evaluate these effects we deposited two series of *a*-Si:H samples. In each series four samples were deposited without breaking the vacuum and each sample was submitted to the gases used for the deposition of the following samples in a series. Furthermore, in order to distinguish between the effects due to the deposition on the freshly deposited samples and the effects due to a contamination of the chamber, the following order of deposition was adopted: (1) deposition of an intrin-

TABLE I. Impurity concentration determined by secondary ion mass spectroscopy in *a*-Si:H samples deposited in different types of reactors.

Type of impurity	Ultrahigh vacuum (UHV)	Type of reactor Monochamber (standard)	ARCAM
O	$2 \times 10^{18}$	$10^{19}$ - $10^{20}$	$5 \times 10^{18}$ - $10^{19}$
C	$4 \times 10^{17}$ - $2 \times 10^{18}$	$10^{19}$ - $10^{20}$	$10^{18}$ - $10^{19}$
N	$5 \times 10^{16}$ - $10^{17}$	$10^{18}$ - $10^{19}$	$< 10^{17}$
Cl	$< 10^{17}$	$10^{16}$ - $10^{17}$	...
F	$< 10^{17}$	...	$< 10^{17}$

insic  $a$ -Si:H film in the  $i$  chamber, (2) deposition of a doped  $p$  ( $n$ ) sample in the  $p$  ( $n$ ) chamber, (3) deposition of an intrinsic  $a$ -Si:H sample in the  $i$  chamber and, (4) deposition of an intrinsic sample in the  $p$  ( $n$ ) chamber. Table II shows the results of dark conductivity ( $\sigma_d$ ) and dark conductivity activation energy ( $E_a$ ) measurements performed on those samples in a coplanar configuration, known to be highly sensitive to surface effects.<sup>27</sup> The values of  $\sigma_d$  and  $E_a$  for an intrinsic  $a$ -Si:H sample are also given. We note that in all cases the chromium contacts were thermally evaporated on the Corning 7059 glass before the  $a$ -Si:H deposition. In the phosphine series, and within the experimental errors, the three intrinsic samples have values of  $\sigma_d$  and  $E_a$  close to the values of the reference sample. From these results we conclude that the exposure of  $a$ -Si:H samples or the walls of the reactor to the silane-phosphine mixture does not produce appreciable effects on the electrical properties of the previously or subsequently deposited  $a$ -Si:H films. On the contrary, for the diborane series we observe that all the "intrinsic" samples have values of  $\sigma_d$  and  $E_a$  differing largely from the values of the reference sample and that  $\sigma_d$  and  $E_a$  depend on the order of the exposure to the gas mixture. Thus, the first sample of the series, exposed to the silane-diborane mixture after its deposition, has  $\sigma_d$  and  $E_a$  values corresponding to a  $p$ -type  $a$ -Si:H sample. On the contrary, the supposed intrinsic  $a$ -Si:H samples deposited in the  $p$  chamber or in the  $i$  chamber exposed to the silane-diborane mixture have  $\sigma_d$  and  $E_a$  values of a slightly boron doped  $a$ -Si:H film, as expected from the SIMS measurements presented in Fig. 5.

To further analyze the effects of the thermal decomposition of diborane we exposed an intrinsic  $a$ -Si:H sample to a 0.2% diborane-silane mixture for 45 min at a total pressure of 5 Pa, followed by the deposition of intrinsic  $a$ -Si:H at 200 °C. Figure 6 shows the results of SIMS measurements performed on this sample; the analysis of the boron concentration profile indicates:

(i) The presence of a boron peak at the interface with the

TABLE II. Dark conductivity and its activation energy measured in a coplanar configuration for two series of  $a$ -Si:H samples produced without the breaking of the vacuum. For all samples, the deposition conditions (standard) were set at a  $T_s$  of 200 °C, an rf power of 10 mW/cm<sup>2</sup>, a silane flow of 15 sccm and a total pressure of 5 Pa. The  $n$ -type ( $p$ -type) doped samples were obtained by an addition of 0.2% phosphine (respectively diborane) to the silane.

Samples	Thickness ( $\mu\text{m}$ )	$E_a$ (eV)	$\sigma_d$ (50 °C) S cm <sup>-1</sup>
Reference	0.70	0.80	$5 \times 10^{-9}$
<b>Phosphine series</b>			
$i$ $a$ -Si:H in $i$ chamber	0.70	0.72	$4 \times 10^{-8}$
$n$ $a$ -Si:H in $n$ chamber	0.61	0.26	$7 \times 10^{-3}$
$i$ $a$ -Si:H in $i$ chamber	0.64	0.80	$1 \times 10^{-8}$
$i$ $a$ -Si:H in $n$ chamber	0.70	0.82	$1 \times 10^{-8}$
<b>Diborane series</b>			
$i$ $a$ -Si:H in $i$ chamber	0.50	0.50	$4 \times 10^{-7}$
$p$ $a$ -Si:H in $p$ chamber	0.98	0.50	$2 \times 10^{-5}$
$i$ $a$ -Si:H in $i$ chamber	0.62	0.95	$4 \times 10^{-11}$
$i$ $a$ -Si:H in $p$ chamber	0.72	1.18	$6 \times 10^{-11}$

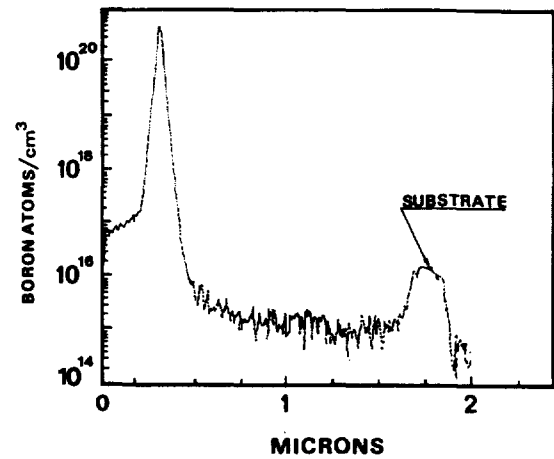


FIG. 6. Boron concentration profile measured by SIMS in a standard  $a$ -Si:H sample deposited at 200 °C, where a boron-contaminated layer, resulting from a 45-min exposure to a flow of 0.2% diborane in silane, was sandwiched between two standard intrinsic plasma deposited  $a$ -Si:H layers.

substrate was systematically observed in SIMS measurements and is associated with the cleaning of the substrate.<sup>28</sup>

(ii) A very low concentration of boron in the bulk of the sample ( $\sim 10^{15}$  B atoms/cm<sup>3</sup>), which proves the high chemical purity and the intrinsic nature of the samples deposited in the ARCAM reactor.

(iii) The presence of a layer containing boron, produced by the chemical vapor deposition (CVD) of the diborane-silane mixture. The boron concentration and the profile of this layer are comparable to those obtained by PECVD.<sup>29</sup> The same boron profile was also obtained by the exposing of  $n$ -type crystalline silicon to  $B_2H_6$  at 830 °C, a method which has been proposed to obtain ultrashallow boron doped layers.<sup>30</sup> As a matter of fact, we have used the CVD of silane-diborane mixtures to produce the  $p$  layer in  $a$ -Si:H based solar cells.<sup>21</sup>

(iv) The effect of the plasma recycling of boron deposited by CVD on the reactor walls and on the substrate itself is shown by the boron profile of the intrinsic layer deposited after the CVD of diborane. This profile is in agreement with the profile obtained on the intrinsic samples deposited in the  $p$  chamber (Fig. 5) and shows again that an intrinsic  $a$ -Si:H cannot be deposited in a boron contaminated chamber.

From the above results it appears that the most important problem in obtaining intrinsic  $a$ -Si:H films arises from the recycling of boron from the walls, unavoidable in monochamber systems. The multiplasma-monochamber system proposed here solves the problem of recycling and thus offers an alternative to the multichamber systems. Though the CVD of diborane can produce serious cross-contamination problems in the fabrication of devices,<sup>31,32</sup> our studies on the CVD of diborane<sup>33-35</sup> showed that its effects are not significant when the time necessary to deposit a  $p$ -type layer is only of a few minutes. Furthermore, a drastic reduction of contamination effects can be obtained by the use of  $B(CH_3)_3$  as a  $p$ -type doping gas.<sup>36,37</sup>

### 3. Abrupt interfaces

From the previous results it appears that the multiplasma system adopted in the ARCAM reactor should be efficient to

produce abrupt interfaces. Moreover, given the volume of the plasma chamber ( $\sim 0.5$  L) and the standard deposition conditions (15 sccm of  $\text{SiH}_4$  at 5 Pa), the residence time of the gases in the plasma chamber is  $\sim 0.1$  s. Then for a typical deposition rate of  $1 \text{ \AA/s}$ , the reduced volume of the deposition chambers (no dead volume), ensures a fast dynamic gas transition of composition and the obtaining of abrupt interfaces. To test the efficiency of the multiplasma system for the production of sharp  $p/i$  interfaces, we compared the external quantum efficiency of two  $p-i-n$  solar cells. Both were produced in the ARCAM reactor under the same plasma conditions. But for one of them the  $p$ ,  $i$ , and  $n$  layers were, respectively, deposited in the  $p$ ,  $i$ , and  $n$  chambers of the ARCAM reactor (multiplasma), whereas for the other the three layers were successively deposited in the same intrinsic chamber (monochamber). Figure 7 shows the spectral quantum efficiency of both devices. The higher blue response achieved in the multiplasma device proves that a better  $p-i$  interface is obtained by the multiplasma system. For comparison, we note that the blue response of  $a\text{-Si:H}$  based solar cells deposited in monochamber systems was improved by the use of a reactive flush with  $\text{NF}_3$  or an hydrogen plasma after the  $p$ -layer deposition.<sup>38,39</sup>

### V. CHARACTERIZATION OF $a\text{-Si:H}$ FILMS DEPOSITED IN THE ARCAM REACTOR

The deposition conditions (pressure, rf power, substrate temperature, flow rate and discharge geometry) for obtaining high quality intrinsic  $a\text{-Si:H}$  films were explored in the ARCAM reactor and the properties of the deposited  $a\text{-Si:H}$  films were fully characterized by a large set of techniques.<sup>21</sup> Moreover, other thin film semiconductors, such as  $\mu\text{c-Si}$ ,  $a\text{-SiGe:H}$ ,  $a\text{-Ge:H}$ ,  $a\text{-SiC:H}$ , and insulators, such as  $a\text{-SiN:H}$ , are being investigated in the ARCAM reactor. We here report results concerning the optimization of the deposition conditions for obtaining a low density of states  $a\text{-Si:H}$ .

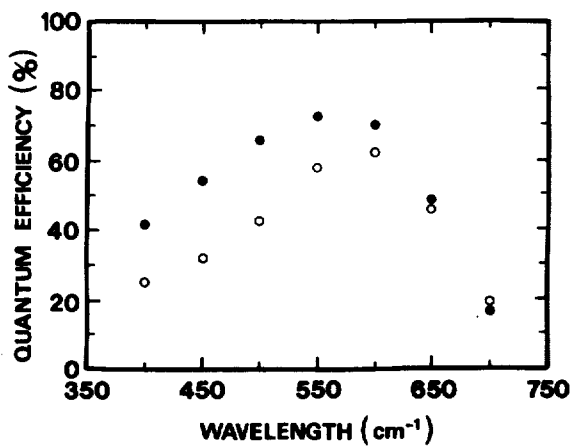


FIG. 7. External quantum efficiency for two  $p-i-n$  solar cells where the three layers were deposited in the same plasma chamber of the ARCAM reactor (open circles) or individually in a different chamber (full circles). The deposition conditions were the same for both devices:  $T_s = 150^\circ\text{C}$ ,  $W_{\text{rf}} = 10 \text{ mW/cm}^2$ ,  $P = 4 \text{ Pa}$ . The  $100 \text{ \AA}$  ( $300 \text{ \AA}$ )  $p$  ( $n$ ) layers were obtained through an addition of 0.2% diborane (phosphine) to the silane. The thickness of the  $i$  layers is  $4000 \text{ \AA}$ .

### A. Electrode geometry and ion bombardment

One parameter often forgotten when comparing the electronic properties of  $a\text{-Si:H}$  films deposited in different laboratories is the reactor geometry. However, the reactor geometry, which can be quantified by the  $S_{\text{rf}}/S_g$  ratio, largely determines the importance of the ion bombardment on the substrates.<sup>40</sup> If we consider an rf discharge with purely capacitive sheaths and a perfectly sinusoidal rf excitation, the plasma potential can be expressed as:<sup>41</sup>

$$V_p = \frac{1}{2} (V_{\text{dc}} + V_{\text{rf}}), \quad (1)$$

where  $V_{\text{dc}}$  and  $V_{\text{rf}}$  are, respectively, the self-bias on the rf electrode and the rf potential. On the other hand, the potential distribution between the rf powered electrode or cathode ( $V_c$ ) and the grounded electrode ( $V_g$ ) is related to the effective area ratio  $S_{\text{rf}}/S_g$  via an inverse power law:<sup>42,43</sup>

$$\frac{V_c}{V_g} = \left( \frac{S_g}{S_{\text{rf}}} \right)^n, \quad (2)$$

where the exponent  $n$  varies from 1 to 4 depending on the rf power. From Eqs. (1) and (2), considering that  $V_{\text{dc}}$  is negative and taking into account that the plasma potential  $V_p$  equals the potential on the grounded electrode  $V_g$  and that  $V_c = V_{\text{dc}} + V_p$ , we obtain:

$$V_{\text{dc}} = V_p \left[ \left( \frac{S_g}{S_{\text{rf}}} \right)^n - 1 \right], \quad (3)$$

and

$$V_p = V_{\text{rf}} \left[ \left( \frac{S_g}{S_{\text{rf}}} \right)^n + 1 \right]^{-1}. \quad (4)$$

From these relations it follows that in the case of a symmetric system ( $S_{\text{rf}} = S_g$ ), the direct-current (dc) self-bias on the rf electrode  $V_{\text{dc}} = 0$  and the plasma potential  $V_p = V_{\text{rf}}/2$ . However, as the ratio  $S_g/S_{\text{rf}}$  increases, the negative dc self-bias increases and the plasma potential (ion energy onto the substrate) decreases. According to this, Fig. 8 shows the variation of  $V_{\text{rf}}$  and  $V_{\text{dc}}$  as functions of the rf power for the two geometries used in the ARCAM reactor.

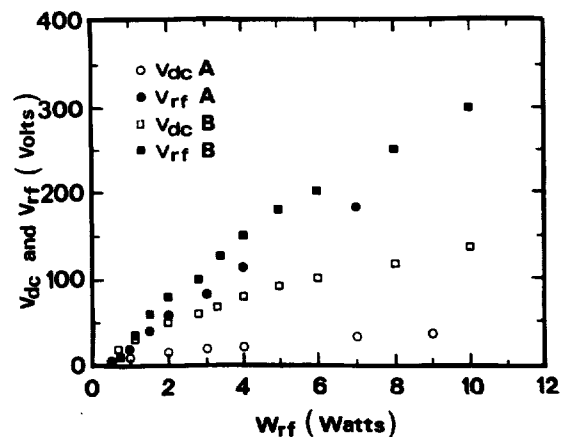


FIG. 8. Radio-frequency potential  $V_{\text{rf}}$  and rf electrode dc self-bias  $V_{\text{dc}}$  as functions of the rf power for the two geometries used in the ARCAM reactor.



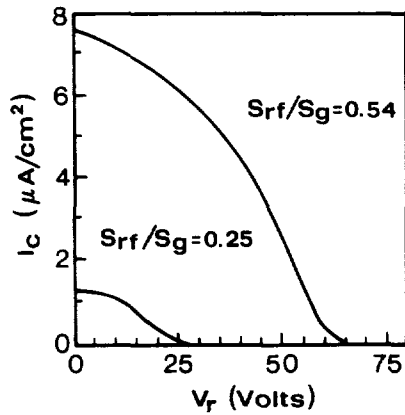


FIG. 9. Ion collector current in an electrostatic analyzer as a function of the retarding potential for two values of the  $S_{rf}/S_g$  area ratio. The plasma conditions are a rf power of 10 mW/cm<sup>2</sup> and a silane pressure of 2 Pa.

We observe that higher values of the negative self-bias  $V_{dc}$  are obtained in the asymmetric system ( $S_{rf}/S_g = 0.25$ ), named geometry *B*. Moreover, measurements of the ion flux and ion energy, performed with an electrostatic energy analyzer on one of the auxiliary reactor systems indicate a large dependence of the ion flux and the ion energy on the reactor geometry. Figure 9 gives the variation of the ion current flux as a function of the retarding potential for two values of the  $S_{rf}/S_g$  ratio. Indeed, the ion current and the ion energy (thus the plasma potential) increase as the  $S_{rf}/S_g$  increases. Further information concerning the characterization of the ion bombardment in rf systems can be found elsewhere.<sup>40</sup>

### B. Effects of the rf power and the gas pressure

Radio-frequency power and gas pressure, being intimately correlated, strongly affect the growth kinetics of *a*-Si:H films. We present in Fig. 10 a complete picture of the rf power dependences of the deposition rate for different silane pressures:

(i) At low pressure (5 Pa) there is a weak dependence of the growth rate as a function of  $W_{rf}$ , independently of the reactor geometry. However, as seen in the previous section, the  $S_{rf}/S_g$  ratio largely affects the ion bombardment. As a consequence we observe that the films deposited in the geometry *A* ( $S_{rf}/S_g = 0.54$ ) tend to peel off from the 7059 Corning glass substrate for  $W_{rf} \geq 3$  W, whereas in the geometry *B* we can increase the rf power up to 10 W without peeling. We relate the higher degree of peeling in the geometry *A* to the stress induced by ion bombardment on the *a*-Si:H films. On the contrary, the density of states of the films deposited at low substrate temperature in the geometry *A* remains below  $10^{16}$  cm<sup>-3</sup> eV<sup>-1</sup>, whereas it is higher when the same discharge conditions are used in geometry *B*. We interpret this as a consequence of the beneficial effects of ion bombardment in reducing the defect density of the films. Indeed, we recently showed that ion bombardment at moderate energies ( $\sim 50$  eV) efficiently reduces the defect density of *a*-Si:H films.<sup>44</sup>

(ii) At high pressure (33 Pa) on the contrary, there is a strong dependence of the growth rate as a function of  $W_{rf}$ . This fast increase of the deposition rate is related to the gam-

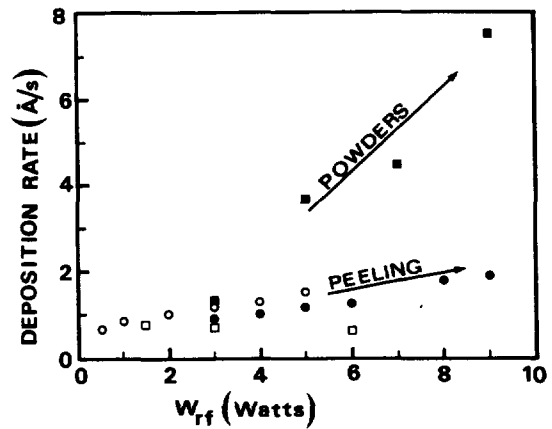


FIG. 10. Variation of the deposition rate as a function of  $W_{rf}$  for different plasma conditions and  $T_s = 200$  °C: open circles are for  $P = 5$  Pa and  $S_{rf}/S_g \sim 0.54$ ; full circles are for  $P = 5$  Pa and  $S_{rf}/S_g \sim 0.25$ ; open squares are for  $P = 20$  Pa and  $S_{rf}/S_g \sim 0.25$ ; and full squares are for  $P = 33$  Pa and  $S_{rf}/S_g \sim 0.25$ . We note that in the low pressure regime (open and full circles) the increase of the  $W_{rf}$  leads to the peeling of the substrates whereas in the high pressure regime (full squares) plasma polymerization and powder formation occur.

ma regime of the rf discharge. We thus observed the existence of two regimes ( $\alpha$  and  $\gamma$ ) in the deposition of *a*-Si:H films from silane discharges.<sup>45</sup> At low pressure ( $\alpha$  regime), the discharge is sustained by the wave riding of electrons which gain energy from the oscillating sheath boundaries and produce ionization and dissociation in the discharge volume. On the contrary, at high pressure ( $\gamma$  regime), there is an increase of the ion-induced secondary electron emission, and ionization and dissociation are dominant within the plasma boundaries. At 33 Pa of pure silane the discharge is in the  $\gamma$  regime, which explains the observed fast increase of the deposition rate with the rf power. But the higher deposition rate achieved in the  $\gamma$  regime generally results in plasma polymerization, powder formation at the exhaust of the deposition chamber and the deposition of a high density of states *a*-Si:H. However, recent results have shown that it is possible to deposit *a*-Si:H with a low density of states even at high deposition rates ( $\gamma$  regime) by the use of a pulsed rf discharge<sup>46</sup> or of a helium dilution of the silane.<sup>47</sup>

(iii) Finally, at intermediate pressures (20 Pa), we observe a decrease of the growth rate as we increase  $W_{rf}$ . This anomalous dependence is explained by the shift of the threshold pressure to higher values as  $W_{rf}$  increases.<sup>45</sup>

### C. Effects of the substrate temperature

Among the process parameters controlling the optoelectronic properties of *a*-Si:H films deposited by rf glow discharge, the substrate temperature is one of the most intensively studied. In general, a low density of states *a*-Si:H is obtained at  $T_s \geq 230$  °C.<sup>48,49</sup> However, our results show that a density of states smaller than  $10^{16}$  cm<sup>-3</sup> and Urbach energies of  $E_0 \leq 60$  meV can be obtained in *a*-Si:H films deposited at 100 °C, provided that the deposition is performed under a moderate ion bombardment (geometry *A*). For typical silane discharge conditions (4 Pa, 15 sccm, and 0.01 W/cm<sup>2</sup>)



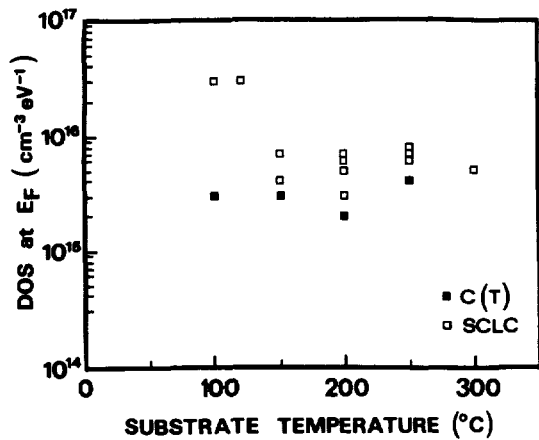


FIG. 11. The Fermi level density of states, measured by SCLC and  $C(T)$  techniques, as a function of the substrate temperature for  $a$ -Si:H films deposited at standard conditions in geometry  $A$ .

the mean ion energy is  $E_{\text{ion}} \sim 20$  eV and the ion flux  $\Phi_{\text{ion}} \sim 10^{12} \text{ cm}^{-2} \text{ s}^{-1}$ , which represents about 2% of the neutral radicals arriving on the substrate.<sup>50</sup> Figure 11 shows the density of states as determined from capacitance versus temperature ( $C$ - $T$ ) experiments carried out at different frequencies<sup>51</sup> and space charge limited current measurements in  $n$ - $i$ - $n$  devices.<sup>50</sup> We note the good agreement between the values of the density of states obtained from these techniques. In Fig. 12 we present the density of states and the Urbach energy deduced from the subgap absorption determined by photothermal deflection spectroscopy measurements (PDS).<sup>52</sup> The density of states obtained by this technique shows the same trend as the one obtained from  $C$ - $T$  and SCLC techniques. However the PDS results are about

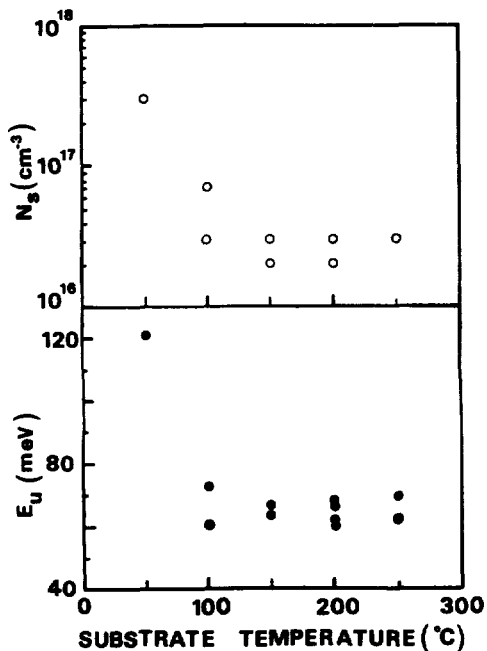


FIG. 12. The density of states  $N_s$  and the Urbach tail energy  $E_u$ , measured by PDS, as functions of the substrate temperature for  $a$ -Si:H films deposited at standard conditions in geometry  $A$ .

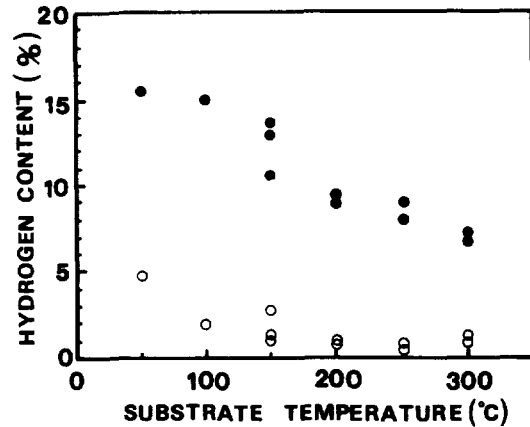


FIG. 13. Hydrogen content as a function of the substrate temperature for  $3\text{-}\mu\text{m}$  thick films deposited at standard conditions in the geometry  $A$ . Full circles give the hydrogen content as deduced from the integrated area under the absorption peak of the Si-H  $630 \text{ cm}^{-1}$  wagging mode, whereas open circles give the hydrogen content as deduced from the integrated area under the absorption peak of the Si-H<sub>2</sub>  $2090 \text{ cm}^{-1}$  stretching mode.

ten times higher, thus indicating an important contribution of the film surfaces to the measured absorption.<sup>53</sup> These results show that the production of low density of states  $a$ -Si:H is possible in a large range of substrate temperatures in a rf glow discharge system. Fig. 12 also shows a sharp increase in both the density of states and Urbach energy when the substrate temperature is reduced down to  $50^\circ\text{C}$ . The ability to produce a low defect density  $a$ -Si:H at low substrate temperatures is of great interest when a thermally activated chemical reaction between substrates and plasma occurs, as for tin-oxide substrates used in large area applications of  $a$ -Si:H.<sup>54</sup>

Even though the density of states of the  $a$ -Si:H films deposited between  $100$  and  $300^\circ\text{C}$  is almost flat, some differences exist between these  $a$ -Si:H films, especially in the hydrogen content which we estimated from the infrared absorption measurements.<sup>55</sup> Figure 13 shows the total hydrogen content determined from the integration of the infrared Si-H wagging band at  $630 \text{ cm}^{-1}$  and the Si-H<sub>2</sub> hydrogen content as determined from the integration of the infrared stretching band at  $2090 \text{ cm}^{-1}$ . The results presented in Fig. 13 show the generally observed decrease of the hydrogen content as the substrate temperature is increased. However, the hydrogen content for the films deposited at low temperature is lower than generally reported for films deposited by rf glow discharge.<sup>56,57</sup> We note that at  $50^\circ\text{C}$  there is a sharp increase of the hydrogen absorption band at  $2090 \text{ cm}^{-1}$ . This is directly related to the increase of the density of states and Urbach energy presented in Fig. 12.

## VI. SUMMARY AND CONCLUSIONS

We have developed a fully automated rf glow discharge system for the deposition of thin film semiconductors and insulators. The specific features of this reactor include the use of an oven-like structure for the heating of the substrate, a dynamic differential pumping, and the use of three independent deposition chambers in the same vacuum vessel.

The evaluation of these features have led us to the following conclusions:

(i) The hot-wall system allows an accurate control of the substrate temperature, which is not affected by the gas pressure or the gas composition as it happens in conventional systems where only the substrate holder is heated. Furthermore the uniform heating of the reactor reduces the outgassing and thus increases the chemical purity of the system. The latter point is enhanced by the use of a dynamic differential pumping which results in a differential pressure between deposition chamber and vacuum vessel, preventing the diffusion of impurities back into the deposition chambers.

(ii) The use of the multiplasma monochamber system proved to be efficient for the production of abrupt interfaces. Indeed the main problem in the production of abrupt interfaces arises from the recycling of the material from the walls. This is effectively avoided in a multiplasma system. On the other hand, the effects of adsorption and thermal decomposition associated with the use of diborane as a *p*-type dopant do not play an important part when the reactive gases are introduced for short periods in the multiplasma system. Moreover these effects can be avoided by the use of  $B(CH_3)_3$  as a *p*-type dopant.

Also, the following results have been obtained from the optimization of the discharge conditions for the deposition of a low density of states *a*-Si:H:

(i) The reactor geometry has a large effect on the ion bombardment, which in turn affects the properties of the *a*-Si:H films. In particular, we found that *a*-Si:H films are highly stressed when deposited in a symmetric geometry. However, the ion bombardment allows to deposit *a*-Si:H films with a low density of states even at 100 °C.

(ii) The deposition rate can be changed by more than one order of magnitude through the adjustment of the gas pressure and rf power even though the increase of the deposition rate generally results in an increase of the *a*-Si:H density of states.

(iii) The substrate temperature does not very much affect the density of states. In particular, *a*-Si:H films with a low density of states ( $<10^{16} \text{ cm}^{-3}$ ) were deposited at  $100 < T_s < 300 \text{ }^\circ\text{C}$ .

In conclusion, the developed fully automated hot-wall multiplasma-monochamber reactor system is perfectly adapted to meet the stringent requirements necessary to the fabrication of amorphous thin films and related devices.

## ACKNOWLEDGMENTS

This work is supported by PIRSEM/CNRS, AFME, TOTAL, and CEC contracts. P. Roca i Cabarrocas thanks AFME for a fellowship. The authors wish to thank D. Conne and M. J. Surmont for their technical assistance, Hoang Xuan Thong for his help in wiring, and R. Morano for his help in developing the software.

<sup>1)</sup> Present address: SOLEMS, 3 rue Léon Blum, F-91124 Palaiseau, Cédex, France.

<sup>1</sup> J. L. Vossen and W. Kern, *Phys. Today*, **33**, No. 5, 26 (1980), and references therein.

<sup>2</sup> For a review see *Plasma Synthesis and Etching of Electronic Materials*, edited by R. P. H. Chang and B. Abeles (Materials Research Society, Pittsburgh, PA, 1984), Vol. 38.

burg, PA, 1984), Vol. 38.

<sup>3</sup> R. C. Chittick, J. H. Alexander, and H. F. Sterling, *J. Electrochem. Soc.* **77**, 116 (1969).

<sup>4</sup> For a recent review see *Amorphous Silicon and Related Materials*, of the series *Advances in Disordered Semiconductors*, edited by Hellmut Fritzsche (World Scientific, Singapore, 1989), Vols. 1 and 2.

<sup>5</sup> See, for example, the *Proceedings of the First International Conference on Amorphous Semiconductor Technology*, edited by M. J. Thompson and D. E. Carlson, Asheville, NC, USA, August 24–25 (Elsevier, Amsterdam, 1989).

<sup>6</sup> For a review see *Semiconductors and Semimetals*, edited by J. I. Pankove (Academic, New York, 1984), Vol. 2, Part A.

<sup>7</sup> Y. Tawada, M. Kondo, H. Okamoto, and Y. Hamakawa, *Sol. Energy Mater.* **6**, 299 (1982).

<sup>8</sup> R. R. Arya, A. Catalano, and R. S. Oswald, *Appl. Phys. Lett.* **49**, 1089 (1986).

<sup>9</sup> A. Asano, T. Ichimura, and H. Sakai, *J. Appl. Phys.* **65**, 2439 (1989).

<sup>10</sup> Y. Kuwano, H. Tarui, T. Takahama, M. Nishikuni, Y. Hishikawa, N. Nakamura, S. Tsuda, S. Nakano, and M. Ohnishi, *J. Non-Cryst. Solids*, **97&98**, 289 (1987).

<sup>11</sup> A. Rothwarf and A. Varonides, in *Proceedings of the 21th IEEE PVSC Conference*, Orlando, Florida, 21–25 May 1990 (to be published).

<sup>12</sup> D. E. Carlson, in *Tetrahedrally Bonded Amorphous Semiconductors*, edited by D. Adler and H. Fritzsche (Plenum, New York, 1985), p. 165.

<sup>13</sup> Y. Marfaing, in *Proceedings of the Second E. C. Photovoltaic Solar Energy Conference* (Reidel, Dordrecht, The Netherlands, 1979), p. 287.

<sup>14</sup> ARCAM stands for Action de Recherche Coordonnée sur les Matériaux Amorphes.

<sup>15</sup> J. Chambouleyron, A. Lloret, P. Roca i Cabarrocas, G. Sardin, and J. Andreu, *Sol. Energy Mater.* **17**, 1 (1988).

<sup>16</sup> Y. Nakayama, T. Ohtsuchi, and T. Kawamura, *J. Appl. Phys.* **62**, 1022 (1987).

<sup>17</sup> *Proceedings of the SERI Photovoltaics Safety Conference*, January 16–17, 1986, Lakewood, CO, USA, published as a special issue of [*Solar Cells* **19** (1987)].

<sup>18</sup> Z. E. Smith, S. Aljishi, D. Slobodin, V. Chu, S. Wagner, P. M. Lenahan, R. R. Arya, and M. S. Bennet, *Phys. Rev. Lett.* **57**, 2450 (1986).

<sup>19</sup> R. A. Street, J. Kakalios, and T. M. Hayes, *Phys. Rev. B* **34**, 3030 (1986).

<sup>20</sup> E. C. Freeman and W. Paul, *Phys. Rev. B* **18**, 4288 (1978).

<sup>21</sup> P. Roca i Cabarrocas, Thèse de l'Université de Paris VII, 1988, in French.

<sup>22</sup> J. P. M. Schmitt, J. Meot, P. Roubeau, and P. Parrons, in *Proceedings of the Eighth E. C. Photovoltaic Solar Energy Conference*, Florence, May 1988 (Kluwer Academic, Dordrecht, The Netherlands, 1988), p. 964.

<sup>23</sup> S. Nakano, S. Tsuda, H. Tarui, T. Takahama, H. Haku, K. Watanabe, M. Nishikuni, Y. Hishikawa, and Y. Kuwano, in *Materials Issues in Applications of Amorphous Silicon Technology*, edited by D. Adler, Y. Hamakawa, and A. Madan (Materials Research Society, Pittsburgh, PA, 1986), Vol. 70, p. 511.

<sup>24</sup> C. C. Tsai, J. C. Knights, and M. J. Thompson, *J. Non-Cryst. Solids* **66**, 45 (1984).

<sup>25</sup> H. Tasaki, W. Y. Kim, M. Hallerdt, M. Konagai, and K. Takahashi, *J. Appl. Phys.* **63**, 550 (1988).

<sup>26</sup> F. Jansen and D. Kuhman, *J. Vac. Sci. Technol. A* **6**, 13 (1988).

<sup>27</sup> M. Tanielian, *Philos. Mag.* **45**, 435 (1982).

<sup>28</sup> G. J. Slusser and L. MacDowell, *J. Vac. Sci. Technol. A* **5**, 1649 (1987).

<sup>29</sup> C. C. Tsai, M. J. Thompson, R. A. Street, M. Stutzman, and F. Ponce, *J. Non-Cryst. Solids* **77&78**, 503 (1985).

<sup>30</sup> J. Nishizawa, K. Aoki, and T. Akamine, *Appl. Phys. Lett.* **56**, 1334 (1990).

<sup>31</sup> R. W. Collins, *Appl. Phys. Lett.* **53**, 1086 (1988).

<sup>32</sup> R. W. Collins and J. M. Cavese, in *Amorphous Silicon Technology*, edited by A. Madan, M. J. Thompson, P. C. Taylor, P. G. LeComber, and Y. Hamakawa (Materials Research Society, Pittsburgh, PA, 1988), Vol. 118, p. 18.

<sup>33</sup> P. Roca i Cabarrocas, A. Labdi, and B. Equer, in *Proceedings of the Eighth E. C. Photovoltaic Solar Energy Conference*, Florence, May 1988 (Kluwer Academic, Dordrecht, The Netherlands, 1988), p. 811.

<sup>34</sup> P. Roca i Cabarrocas, Satyendra Kumar, and B. Drevillon, *J. Appl. Phys.* **66**, 3286 (1989).

<sup>35</sup> P. Roca i Cabarrocas, Satyendra Kumar, and B. Drevillon, in *Proceedings of the Ninth E. C. Photovoltaic Solar Energy Conference*, Freiburg, Sep-

- tember 1989 (Kluwer Academic, Dordrecht, The Netherlands, 1989), p. 263.
- <sup>36</sup>W. Zongyan, A. Lloret, J. M. Siefert, P. Roca i Cabarrocas, and B. Equer, in *Amorphous Silicon Technology*, edited by A. Madan, M. J. Thompson, P. C. Taylor, Y. Hamakawa, and P. G. LeComber (Materials Research Society, Pittsburgh, PA, 1989), Vol. 149, p. 291.
- <sup>37</sup>H. Tarui, T. Matsuyama, S. Okamoto, Y. Hishikawa, H. Dohjo, N. Nakamura, S. Tsuda, S. Nakano, M. Ohnishi, and Y. Kuwano, in *Technical Digest of the International PVSEC-4*, Sydney, Australia (1987).
- <sup>38</sup>A. Catalano and G. Wood, *Appl. Phys. Lett.* **63**, 1220 (1988).
- <sup>39</sup>Y. S. Tsuo, Y. Xu, R. S. Crandall, H. S. Ullal, and K. Emery, in *Amorphous Silicon Technology*, edited by A. Madan, M. J. Thompson, P. C. Taylor, Y. Hamakawa, and P. G. LeComber (Materials Research Society, Pittsburgh, PA, 1989), Vol. 149, p. 471.
- <sup>40</sup>P. Roca i Cabarrocas, in *Amorphous Silicon Technology*, edited by A. Madan, M. J. Thompson, P. C. Taylor, Y. Hamakawa, and P. G. LeComber (Materials Research Society, Pittsburgh, PA, 1989), Vol. 149, p. 33.
- <sup>41</sup>B. Chapman, in *Glow Discharge Processes, Sputtering and Plasma Etching* (Wiley, New York, 1980), p. 168.
- <sup>42</sup>H. R. Konig and L. I. Maissel, *IBM J. Res. Develop.* **14**, 168 (1970).
- <sup>43</sup>A. M. Pointu, *Appl. Phys. Lett.* **50**, 1047 (1987).
- <sup>44</sup>P. Roca i Cabarrocas, P. Morin, J. Conde, V. Chu, J. Z. Liu, H. R. Park, and S. Wagner, in *Amorphous Silicon Technology*, Proceedings of the Materials Research Society 1990 Spring Meeting, San Francisco, (to be published).
- <sup>45</sup>J. Perrin, P. Roca i Cabarrocas, B. Allain, and J. M. Friedt, *Jpn. J. of Appl. Phys.* **27**, 2041 (1988).
- <sup>46</sup>A. Lloret, E. Bertran, J. L. Andujar, A. Canillas, and J. L. Morenza, *J. Appl. Phys.* (submitted).
- <sup>47</sup>P. Roca i Cabarrocas (to be published).
- <sup>48</sup>D. E. Carlson, *Prog. Cryst. Growth Charact.* **4**, 173 (1981).
- <sup>49</sup>I. Solomon, R. Benferhat, and H. Tran-Quoc, *Phys. Rev. B* **30**, 3422 (1984).
- <sup>50</sup>P. Roca i Cabarrocas, A. M. Antoine, B. Drevillon, and J. P. M. Schmitt, in *Proceedings of the Seventh International Symposium on Plasma Chemistry*, edited by C. J. Timmermans, (IUPAC, Eindhoven, The Netherlands, 1985) p. 136.
- <sup>51</sup>K. Zellama, J. D. Cohen, and J. P. Harbison, in *Materials Issues in Applications of Amorphous Silicon Technology*, edited by D. Adler, A. Madan, and M. J. Thompson (Materials Research Society, Pittsburgh, PA, 1985), Vol. 49, p. 311.
- <sup>52</sup>W. B. Jackson, N. M. Amer, A. C. Boccara, and D. Fournier, *Appl. Opt.* **20**, 1333 (1981).
- <sup>53</sup>Z. E. Smith, V. Chu, K. Shepard, S. Aljishi, D. Slobodin, J. Kolodzey, and S. Wagner, *Appl. Phys. Lett.* **50**, 1521 (1987).
- <sup>54</sup>B. Drevillon, S. Kumar, and P. Roca i Cabarrocas, *Appl. Phys. Lett.* **54**, 2088 (1989).
- <sup>55</sup>H. Sanks, C. J. Fang, L. Ley, M. Cardona, F. J. Demond, and S. Kalbitzer, *Phys. Stat. Sol. B* **100**, 43 (1980).
- <sup>56</sup>A. Matsuda, in *Proceedings of the 10th ISIAT*, Tokyo, 1986 (unpublished), p. 331.
- <sup>57</sup>H. Fritzsche, M. Tanielian, C. C. Tsai, and P. J. Gaczi, *J. Appl. Phys.* **50**, 3366 (1979).